Article

Neuron

Cell-Type-Specific Activity in Prefrontal Cortex during Goal-Directed Behavior

Highlights

- Sensory, motor, outcome signals are found in mouse PFC during goal-directed behavior
- Inhibitory neurons of the same subtype show similar functional properties
- Different subtypes of PFC inhibitory neurons encode different task-related signals
- Excitatory neurons are diverse and their task-related activity varies across layers

Authors

Lucas Pinto, Yang Dan

Correspondence

ydan@berkeley.edu

In Brief

Cellular-resolution Ca^{2+} imaging from the mouse PFC during goal-directed behavior reveals sensory, motor, and outcome signals. Interneurons of the same subtype are functionally similar, but different subtypes encode different task-related signals. Excitatory neurons have diverse properties that vary across layers.

Pinto & Dan, 2015, Neuron *87*, 437–450
July 15, 2015
http://dx.doi.org/10.1016/j.neuron.2015.06.021

CellPress

Neuron
Article

Cell-Type-Specific Activity in Prefrontal Cortex during Goal-Directed Behavior

Lucas Pinto[1] and Yang Dan[1,*]
[1]Division of Neurobiology, Department of Molecular and Cell Biology, Helen Wills Neuroscience Institute, Howard Hughes Medical Institute, University of California, Berkeley, Berkeley, CA 94720, USA
*Correspondence: ydan@berkeley.edu
http://dx.doi.org/10.1016/j.neuron.2015.06.021

SUMMARY

The prefrontal cortex (PFC) plays a key role in controlling goal-directed behavior. Although a variety of task-related signals have been observed in the PFC, whether they are differentially encoded by various cell types remains unclear. Here we performed cellular-resolution microendoscopic Ca^{2+} imaging from genetically defined cell types in the dorsomedial PFC of mice performing a PFC-dependent sensory discrimination task. We found that inhibitory interneurons of the same subtype were similar to each other, but different subtypes preferentially signaled different task-related events: somatostatin-positive neurons primarily signaled motor action (licking), vasoactive intestinal peptide-positive neurons responded strongly to action outcomes, whereas parvalbumin-positive neurons were less selective, responding to sensory cues, motor action, and trial outcomes. Compared to each interneuron subtype, pyramidal neurons showed much greater functional heterogeneity, and their responses varied across cortical layers. Such cell-type and laminar differences in neuronal functional properties may be crucial for local computation within the PFC microcircuit.

INTRODUCTION

Goal-directed behavior involves multiple sensory, motor, and cognitive processes. When engaged in a task, the animal must attend to task-relevant sensory cues, control the initiation and termination of appropriate motor actions, and monitor the outcome of each action in order to adjust future behavioral strategies. The prefrontal cortex (PFC) plays a crucial role in coordinating these processes through its long-range connections with many other brain areas (Desimone and Duncan, 1995; Euston et al., 2012; Fuster, 2008; Gabbott et al., 2005; Heidbreder and Groenewegen, 2003; Miller and Cohen, 2001; Squire et al., 2013). Electrophysiological recordings from both primates and rodents have shown that a variety of task-related signals are encoded in the spiking activity of PFC neurons (Euston et al., 2012; Miller and Cohen, 2001). In addition to sensory stimuli and impending motor actions, many neurons respond to expected or actual action outcomes (reward and punishment), thus allowing the PFC to orchestrate sensory and motor processes for the current task and to improve future behavioral performance (Hayden et al., 2008; Hyman et al., 2013; Insel and Barnes, 2014; Ito et al., 2003; Matsumoto et al., 2007; Narayanan et al., 2013; Ridderinkhof et al., 2004; Schall et al., 2002; Wallis and Kennerley, 2010; Watanabe, 1996).

Individual PFC neurons encode various combinations of task-related variables (Hyman et al., 2013; Machens et al., 2010; Mante et al., 2013; Rigotti et al., 2013), exhibiting a high degree of complexity and heterogeneity. How these functional properties are organized and computed within the PFC microcircuit remains largely unknown. In well-studied sensory cortical areas, glutamatergic neurons and subtypes of GABAergic interneurons exhibit different stimulus selectivity (Kerlin et al., 2010), and they are differentially influenced by brain state and neuromodulatory inputs (Alitto and Dan, 2012; Fu et al., 2014; Gentet et al., 2012; Lee et al., 2013; Pi et al., 2013; Zhang et al., 2014), suggesting separate roles in local computation. However, how different types of neurons in the PFC respond to task-related events is only beginning to be investigated (Courtin et al., 2014; Kvitsiani et al., 2013; Sparta et al., 2014). Furthermore, a prominent feature of the neocortex is its laminar organization. Neurons in different layers receive different inputs and project to distinct targets, and their interconnections play crucial roles in intracortical processing (Douglas and Martin, 2004; Harris and Mrsic-Flogel, 2013). Characterizing the laminar organization of neuronal response properties is thus a critical step in understanding how the PFC circuit operates in cognitive control.

In this study, we characterized PFC activity while the mouse performed a simple go/no-go sensory discrimination task, which has been used extensively to study PFC functions (Fuster, 2008). The use of microendoscopes (Ghosh et al., 2011) allowed optical access to the dorsomedial PFC (dmPFC), a region important for cognitive control of behavior (Bissonette et al., 2008; Euston et al., 2012; Hanks et al., 2015; Matsumoto et al., 2007; Narayanan et al., 2013; Ridderinkhof et al., 2004) but inaccessible to conventional imaging techniques. Using several Cre mouse lines, we performed cellular-resolution Ca^{2+} imaging from excitatory pyramidal (PYR) neurons as well as three distinct subtypes of inhibitory interneurons: parvalbumin-positive (PV^+), somatostatin-positive (SST^+), and vasoactive intestinal peptide-positive (VIP^+) neurons, which together comprise 85% of all GABAergic neurons in the cortex (Rudy et al., 2011; Xu et al.,

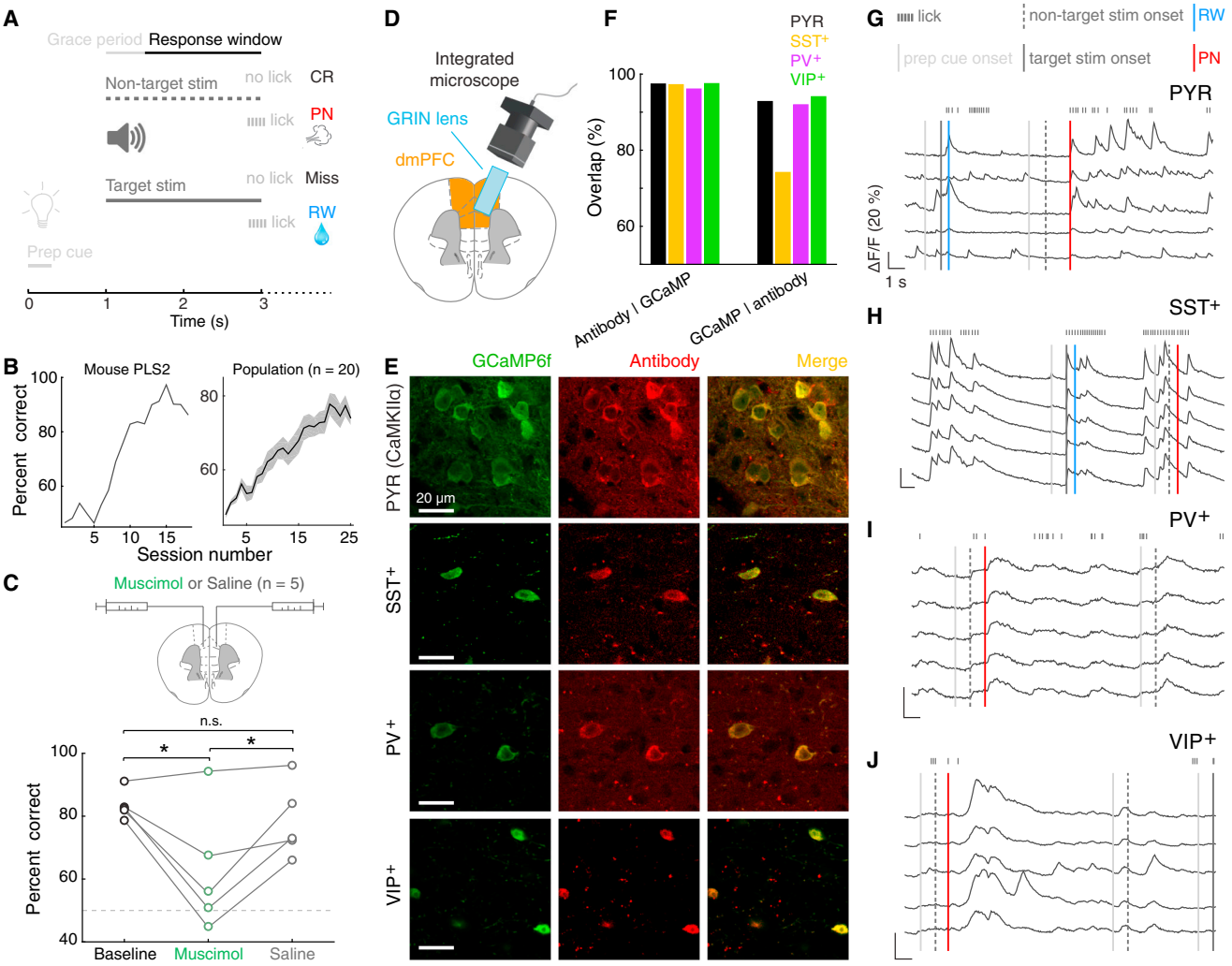

Figure 1. Experimental Approach

(A) Schematic of the behavioral task.

(B) Learning curves of an example mouse (left) and population of imaged mice (right, n = 20). The surgery for GRIN lens implantation happened between sessions 2 and 11 (5.8 ± 3.6, mean ± SD), and it did not seem to affect learning of the task. Line, mean; shaded area, ±SEM.

(C) Bilateral muscimol injections in dmPFC reversibly impaired task performance. Lines correspond to individual mice. Dashed horizontal line, chance performance. *$p < 0.05$; n.s., not significant.

(D) Schematic of GRIN lens implanted in dmPFC.

(E) Example of GCaMP6f expression and immunostaining for cell-type-specific marker for each cell type.

(F) Cell-type specificity and efficiency of GCaMP6f expression. PYR (CAMKIIα): 97.4% (2,313/2,375) of GCaMP6f-expressing cells were CAMKIIα+, n = 3 mice; PV$^+$: 96.1% (342/356), n = 2; SST$^+$: 97.2% (522/537), n = 2; VIP$^+$: 97.5% (348/357), n = 3; conversely, 92.8%, 74.1%, 91.3%, and 94.0% of antibody-labeled cells expressed GCaMP6f for PYR, SST$^+$, PV$^+$, and VIP$^+$ neurons, respectively.

(G–J) Fluorescence (ΔF/F) traces of example PYR (G), SST$^+$ (H), PV$^+$ (I), and VIP$^+$ (J) neurons while each animal performed the task. The neurons shown in each plot were simultaneously recorded. Vertical lines of different types and colors represent different task-related events.

See also Figure S1.

2010). For inhibitory interneurons, we found a high degree of functional similarity within each subtype but clear distinction between subtypes. Pyramidal neurons showed diverse responses to task-related events, and their heterogeneity was partly attributable to functional variations across cortical layers. These results provide the first comprehensive characterization of PFC microcircuit activity during a commonly studied goal-directed behavior.

RESULTS

A dmPFC-Dependent Go/No-Go Task

We trained head-fixed mice on a go/no-go auditory discrimination task (Figure 1A, see Experimental Procedures). The start of each trial was signaled by a light flash, followed by presentation of either the target (17 kHz) or non-target (9 kHz) auditory stimulus. After a grace period of 500 ms (during which licking

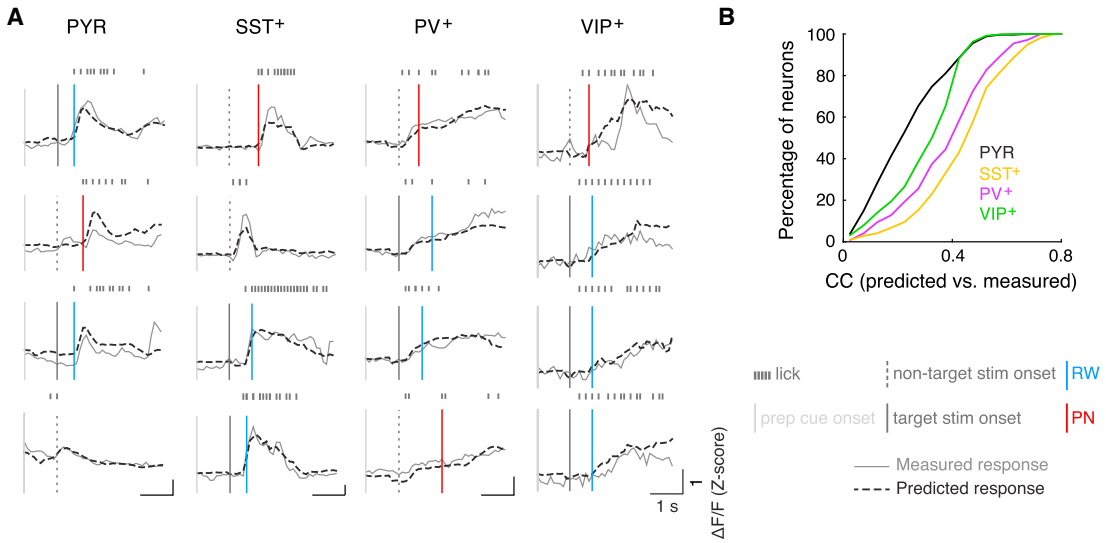

Figure 2. Performance of the GLM

(A) Fluorescence traces measured in several example trials for an example neuron of each cell type (solid gray lines), and those predicted by the GLM (dashed black lines). Data from these trials were not used to fit the model.

(B) Cumulative distribution of CCs for task-modulated neurons of each type (n = 631, 388, 243, and 390 for PYR, SST^+, PV^+, and VIP^+ neurons, respectively).

had no consequence), licking in response to the target tone (hit) was rewarded with water, while licking to the non-target tone (false alarm) was punished by an airpuff and time-out. Mice learned this task within days (Figure 1B), but their performance did not reached 100%, allowing us to observe dmPFC activity during both correct and error trials.

To test the involvement of dmPFC in this task, we suppressed the neuronal activity pharmacologically. Bilateral injections of the $GABA_A$ receptor agonist muscimol, but not saline, resulted in a marked but reversible decrease in task performance (Figure 1C, $p = 0.01$, $F_{2,4} = 8.21$, one-way repeated-measures ANOVA, $n = 5$; muscimol versus baseline: $p = 0.01$, muscimol versus saline: $p = 0.04$, saline versus baseline: $p = 0.63$, Tukey's post hoc test). This effect was not due to a general motor deficit, since licking was unaffected when the mouse was given free access to water (Figure S1A; $p = 0.55$, paired t test, $n = 5$). Thus, normal dmPFC activity is required for the go/no-go auditory discrimination task.

Task-Related Activity of Different Cell Types

To image pyramidal neurons and each interneuron subtype, we injected adeno-associated virus (AAV) into the dmPFC of CaMKIIα-, PV-, SST-, or VIP-Cre mice for Cre-inducible expression of the Ca^{2+} indicator GCaMP6f (Chen et al., 2013b). Immunohistochemical staining confirmed the specificity of GCaMP6f expression (Figures 1E and 1F). We performed Ca^{2+} imaging through a gradient refractive index (GRIN) lens coupled to a miniaturized integrated fluorescence microscope (Figures 1D and S1B and Movie S1)(Ghosh et al., 2011), which allowed us to monitor dmPFC activity across cortical layers with cellular resolution (medial → lateral, superficial → deep layers).

All cell types exhibited Ca^{2+} transients associated with task-related events (Figures 1G–1J). However, the percentage of neurons that were significantly modulated by the task ($p < 0.01$, three-way ANOVA, see Experimental Procedures) differed across cell types, higher for PV^+ (95.3%) and SST^+ (96.9%) than for VIP^+ (81.2%) and PYR (77.3%) neurons (Figure S1C, $p = 7.8 \times 10^{-16}$, χ^2 test).

Generalized Linear Model

We next analyzed the activity of each cell type associated with each task-related event. To disambiguate the contributions of different task-related events to the activity of each neuron, we fitted its Ca^{2+} activity using a generalized linear model (GLM) with all events as regressors (see Supplemental Experimental Procedures). The performance of each model was measured by the correlation coefficient (CC) between the predicted and measured activity using a separate test dataset not used for fitting the model (Figure 2A). Among neurons that were significantly modulated by the task (Figure S1C), the average CCs were higher for SST^+ (0.46 ± 0.01, mean ± SEM, $n = 388$) and PV^+ (0.40 ± 0.01, $n = 243$) than for VIP^+ (0.31 ± 0.01, $n = 390$) and PYR neurons (0.24 ± 0.01, $n = 631$) (Figure 2B, $p = 2.5 \times 10^{-99}$, $F_{3,1648} = 176.7$, one-way ANOVA; $SST^+ > PV^+ > VIP^+ > PYR^+$, $p < 0.001$ for all comparisons, Tukey's post hoc test). Thus, the activity of SST^+ and PV^+ neurons was not only more modulated by the task (Figure S1C) but also better described by a linear model based on task-related events. We next compared the activity associated with each task-related event across cell types.

Sensory-Related Activity

Goal-directed behavior depends on the processing of task-related sensory cues. Two sensory cues are relevant to the current task: the light flash at trial start, which serves as a preparatory ("prep") signal, and the auditory stimulus ("stim"), which instructs the appropriate motor action (go or no-go, Figure 3A). As shown by event-triggered average of the fluorescence signals (Figures 3B–3E and 3J), the prep cue triggered small but

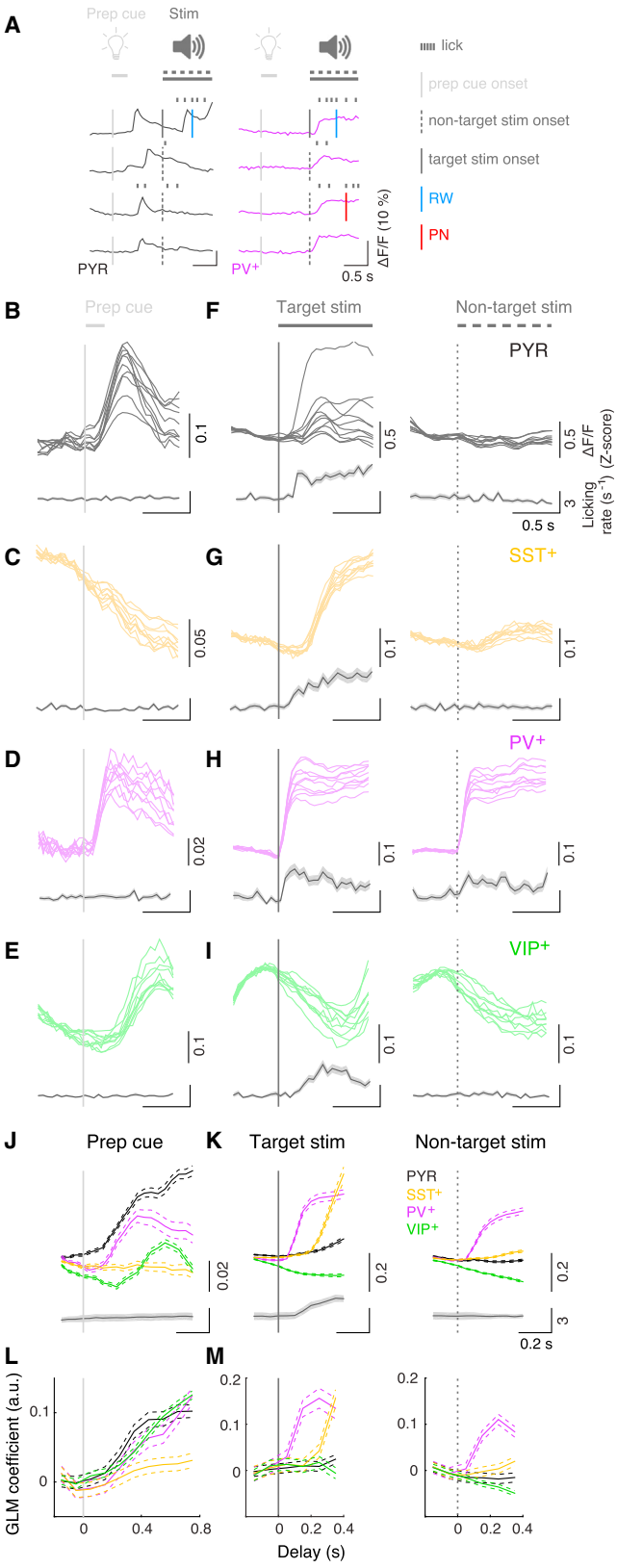

Figure 3. Sensory-Related Activity

(A) Example ΔF/F traces of a PYR (left) and a PV$^+$ (right) neuron (4 trials each) around the time of sensory cues (prep cue and stim).

(B–E) Trial-averaged ΔF/F traces at prep cue (gray vertical line) from a representative PYR (B), SST$^+$ (C), PV$^+$ (D), and VIP$^+$ (E) recording. Each plot shows the trial-averaged responses of 10 example neurons recorded simultaneously in the same field of view (top, thin colored lines), along with corresponding licking rate histograms (bottom, gray lines and shaded areas, mean ± SEM).

(F–I) Trial-averaged ΔF/F traces at the target (left) and non-target (right) auditory stimulus onset for the same neurons shown in (B)–(E), with corresponding licking rate histograms.

(J) Top: population average of prep cue responses averaged across all task-modulated neurons of each type (PYR: n = 631; SST$^+$: n = 388; PV$^+$: n = 243; VIP$^+$: n = 390). Bottom: average licking rate triggered by prep cue (n = 104 sessions, 20 mice). Thick lines, mean; thin dashed lines, ±SEM.

(K) Population average of responses to target and non-target stimuli averaged across all task-modulated neurons of each type.

(L) GLM coefficients for prep cue averaged across all task-modulated neurons of each type with statistically significant fits (see Supplemental Experimental Procedures, PYR: n = 604; SST$^+$: n = 385; PV$^+$: n = 242; VIP$^+$: n = 370). Thick lines, mean; thin dashed lines, ±SEM.

(M) GLM coefficients for target (left) and non-target (right) stimuli averaged across each cell type.

See also Figure S2.

detectable responses in PYR, PV$^+$, and VIP$^+$ neurons, but rarely in SST$^+$ neurons.

We next analyzed the responses to target and non-target auditory stimuli separately. The target stimulus evoked responses in many PYR, PV$^+$, and SST$^+$ cells but not in VIP$^+$ cells (Figures 3F–3I and 3K, left column), while the non-target stimulus evoked consistent responses only in PV$^+$ neurons (right column). However, such preferential responses to the target stimulus could be related to the impending motor action, since well-trained mice are much more likely to lick following the target than non-target stimulus. To test this possibility, we analyzed the responses of each neuron in trials with or without licking immediately following each auditory stimulus (Figure S2). For both PYR and SST$^+$ neurons, the Ca^{2+} signals were primarily associated with licking, since in trials without immediate licking there was no significant response to either the target or non-target stimulus ($p > 0.5$, one-sided signed-rank test). In contrast, many PV$^+$ cells responded to both stimuli at short latencies regardless of licking (Figures 1I, 3A, and S2C, $p = 2.8 \times 10^{-14}$ for trials without licking). Thus, PV$^+$ neurons appear to be unique in their responses to the auditory stimuli.

We then compared the GLM coefficients for each regressor across cell types. Consistent with the event-triggered average analysis, PYR, PV$^+$ and VIP$^+$ cells all showed higher prep cue coefficients than SST$^+$ neurons (Figure 3L, $p = 5.9 \times 10^{-19}$, $F_{3,1597} = 30.1$, one-way ANOVA; $p < 0.001$ for all post hoc comparisons, Tukey's test), and PV$^+$ neurons constituted the only cell type with short-latency auditory responses (Figure 3M, $p = 8.2 \times 10^{-31}$, one-sided signed-rank test).

Motor-Related Activity

Goal-directed behavior inevitably involves motor action, which consists of licking in the current task. Analysis of this behavior showed that most of the licks were organized in bouts, with short inter-lick intervals within each bout and long intervals between bouts (Figure S3). We found that all cell types exhibited

licking-related activity (Figures 1G–1J), consistent with the known role of dmPFC in action selection and its strong connections with motor circuits (Euston et al., 2012; Gabbott et al., 2005; Heidbreder and Groenewegen, 2003; Hyman et al., 2013). Interestingly, most neurons showed higher activity at the beginning and end of each bout than in the middle (Figure 4A), reminiscent of the previous finding that PFC neurons preferentially signal boundaries of action sequences (Fujii and Graybiel, 2003). We thus analyzed the Ca^{2+} activity of each neuron at both lick-bout onset and offset.

We found the most striking licking-related activity in SST^+ neurons, regardless of whether the lick bout occurred within a trial or during an inter-trial interval (Figure 1H). The activity increased consistently at bout onset and sometimes also at bout offset (Figures 1H, 4A, 4C, 4F, and 4G). PV^+ neuron activity was also strongly correlated with both onset and offset of licking (Figures 4D, 4F, and 4G). The activity of PYR cells was highly diverse, exhibiting different amplitudes and temporal profiles at licking onset and offset (Figure 4B). Interestingly, VIP^+ cells showed consistent Ca^{2+} increases at licking offset but not at onset (Figures 4A and 4E–4G).

Analysis of the GLM coefficients revealed that, at lick-bout onset, SST^+ neurons showed by far the strongest activity and VIP^+ neurons the weakest (Figure 4H, $p = 2.9 \times 10^{-134}$, $F_{3,1597} = 252.9$, one-way ANOVA; SST^+ and VIP^+: $p < 10^{-10}$ versus other types, PV^+ versus PYR: $p = 0.58$, Tukey's post hoc test). In contrast, at lick-bout offset, VIP^+ neurons showed the strongest activity (Figure 4I, $p = 7.8 \times 10^{-80}$, $F_{3,1597} = 138.6$, one-way ANOVA; VIP^+: $p < 10^{-5}$ versus all other types, Tukey's post hoc test).

Outcome-Related Activity

Previous studies in monkeys and rats indicate that outcome-related activity is widespread in the PFC (Hayden et al., 2008; Hyman et al., 2013; Insel and Barnes, 2014; Ito et al., 2003; Matsumoto et al., 2007; Narayanan et al., 2013; Schall et al., 2002; Wallis and Kennerley, 2010). Here we observed responses to both reward ("RW," water drop following hit) and punishment ("PN," airpuff and time-out following false alarm). Strong outcome-related activity was observed in many VIP^+ and PV^+ neurons (Figures 5D–5G). It was also observed in many PYR cells (Figures 5A and 5B), but with a high degree of heterogeneity with respect to response amplitude and time course (Figure 5B). In contrast, SST^+ neurons showed little outcome-related activity (Figure 5C); although many cells exhibited Ca^{2+} transients following RW or PN, they appeared to be associated with licking (Figure S4).

To further disambiguate licking- and outcome-related activity, we examined the GLM coefficients for both outcomes. Significant PN responses were found in VIP^+, PV^+, and PYR neurons (Figure 5I; $p < 10^{-10}$, signed-rank test), but not in SST^+ neurons ($p = 0.61$), while RW responses were larger in PV^+ neurons than all other cell types (Figure 5H, $p = 1.5 \times 10^{-8}$, $F_{(3,1597)} = 13.2$, one-way ANOVA; $p < 0.01$ for comparison between PV^+ and all other cell types, Tukey's post hoc test). Consistent with previous reports (Hyman et al., 2013; Matsumoto et al., 2007), the responses to PN were stronger than those to RW for PYR ($p = 8.4 \times 10^{-16}$, signed-rank test), PV^+ ($p = 2.5 \times 10^{-4}$), and VIP^+ neurons ($p = 3.7 \times 10^{-31}$), although not for SST^+ cells ($p = 0.88$).

In sum, these results demonstrate clear distinctions among the interneuron subtypes: SST^+ neurons showed the strongest motor-related activity but little sensory- or outcome-related activity, whereas PV^+ neurons responded to all task-related events (sensory, motor, and outcome). Although VIP^+ neurons showed strong activity at both PN and lick-bout offset (Figures 4I and 5I), the offset activity was powerfully gated by PN (see below), indicating a predominant effect of action outcome in controlling VIP^+ neuron activity.

Modulation of dmPFC Activity by Action Outcome

An important component of cognitive control is to adjust behavioral strategies based on recent action outcomes (Ridderinkhof et al., 2004; Schall et al., 2002). In our study, performance of the mice following false alarm-triggered punishment was significantly better than that following reward, primarily due to a reduced false alarm rate (Figure 6A, percent correct: $p = 0.003$; hit rate: $p = 0.34$; false alarm rate: $p = 1.7 \times 10^{-4}$, paired t test, $n = 20$ mice). This indicates that a negative outcome can trigger behavioral adjustments to avoid the same mistake.

The rodent PFC is known to be required for such behavioral adjustments (Narayanan et al., 2013). To identify potential neural correlates of this adjustment in the dmPFC, we analyzed the trials immediately following punishment (post-PN) and those following reward (post-RW) separately (see Supplemental Experimental Procedures). For PYR and VIP^+ cells, responses to the prep cue were much larger in post-PN trials (Figures 6B and 6C, $p < 10^{-6}$ for both cell types, signed-rank test), whereas the opposite was true for PV^+ neurons (Figure 6C, $p = 8.2 \times 10^{-8}$). These differences were not caused by different licking behaviors in post-PN and post-RW trials, because only trials with no licking within 1 s after the prep cue onset were included in the analysis. They were also not caused by different pre-trial baseline activity, since even when we selected trials with matched baseline activity, similar differences between post-PN and post-RW trials were still observed (Figure S5). Such cell-type-specific modulation of PFC responses to the prep cue, especially the enhanced activity of PYR neurons, could contribute to the improved cognitive control following error trials (Hayden et al., 2008; Narayanan et al., 2013; Ridderinkhof et al., 2004).

In addition to enhancing activity in the following trial, we also noticed a more immediate modulatory effect of PN. For all cell types, licking offset was followed by a much greater Ca^{2+} increase if it occurred within 2 s of the false alarm-triggered airpuff than at other times (Figures 6D and 6E, $p < 0.05$ for all types, signed-rank test). Thus, besides evoking direct neuronal responses (Hayden et al., 2008; Hyman et al., 2013; Insel and Barnes, 2014; Ito et al., 2003; Matsumoto et al., 2007; Narayanan et al., 2013; Schall et al., 2002; Wallis and Kennerley, 2010), action outcomes also strongly modulate the responses to subsequent task-related events.

Spatial Organization of Response Properties

To characterize the spatial organization of task-related neuronal activity, we first computed the CC between the fluorescence traces of each pair of neurons within each field of view and plotted the CC against the distance between the cell pair. Within

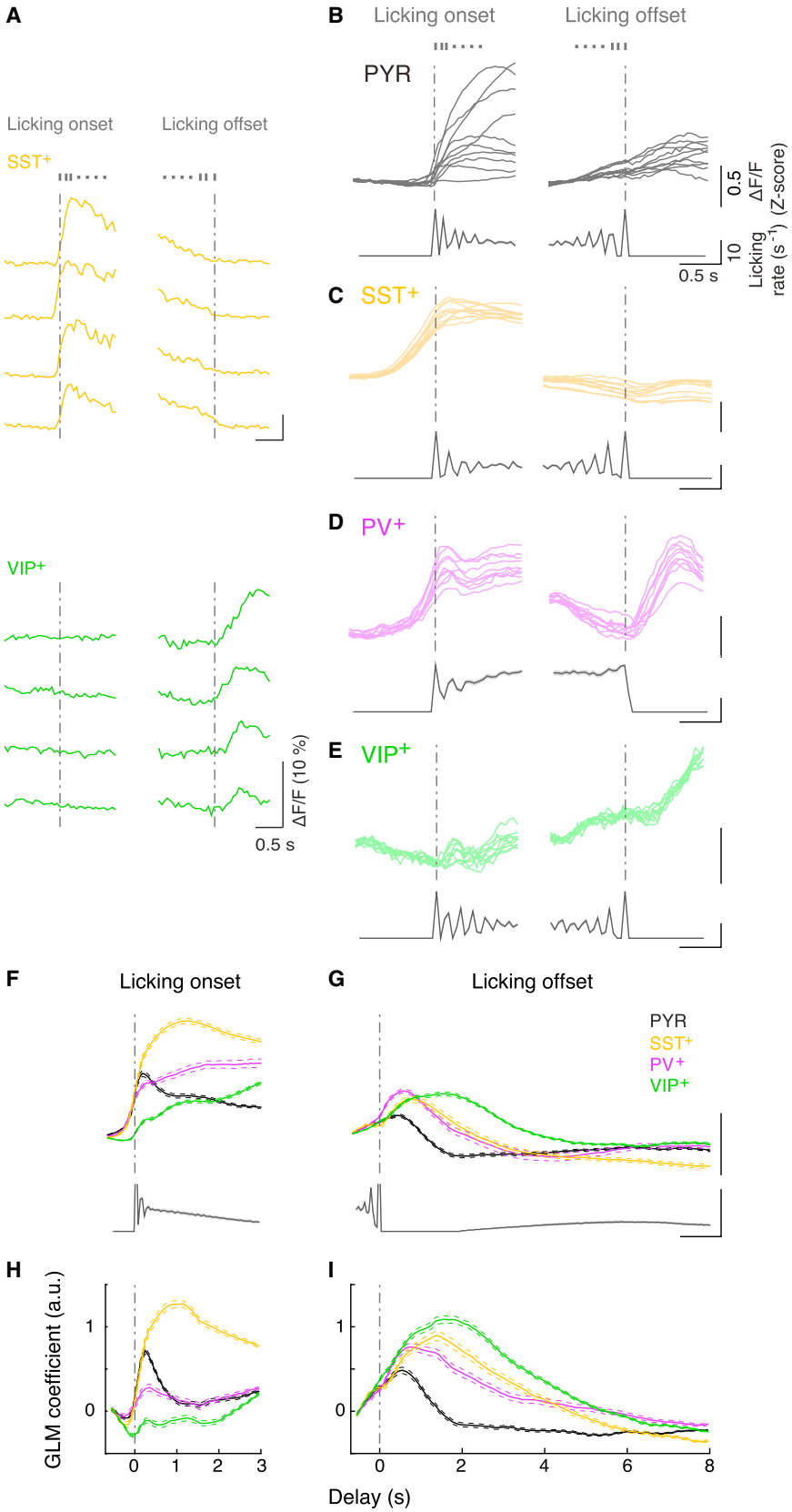

Figure 4. Motor-Related Activity

(A) ΔF/F traces of an SST$^+$ (top) and a VIP$^+$ (bottom) neuron at onset (left) and offset (right) of several example licking bouts.

(B–E) Trial-averaged ΔF/F traces at lick-bout onset (left) and offset (right) from a representative recording for each cell type. Each plot contains trial-averaged responses of 10 example neurons recorded simultaneously in the same field of view (top, thin colored lines), with corresponding licking rate histograms (bottom). The same neurons are shown on the left and right plots. Note that all licking bouts were included in this analysis, regardless of when they occurred in the trial.

(F and G) Top: population average of responses to licking onset (F) and offset (G) averaged across all significantly modulated cells of each type. Bottom: population average of licking histograms (truncated for the bin at t = 0 since by definition there is always a lick in that bin). Thick lines, mean; thin dashed lines, ±SEM.

(H and I) GLM coefficients for licking onset (H) and offset (I) averaged across each cell type. Thick lines: mean, thin dashed lines: ± SEM.

See also Figure S3.

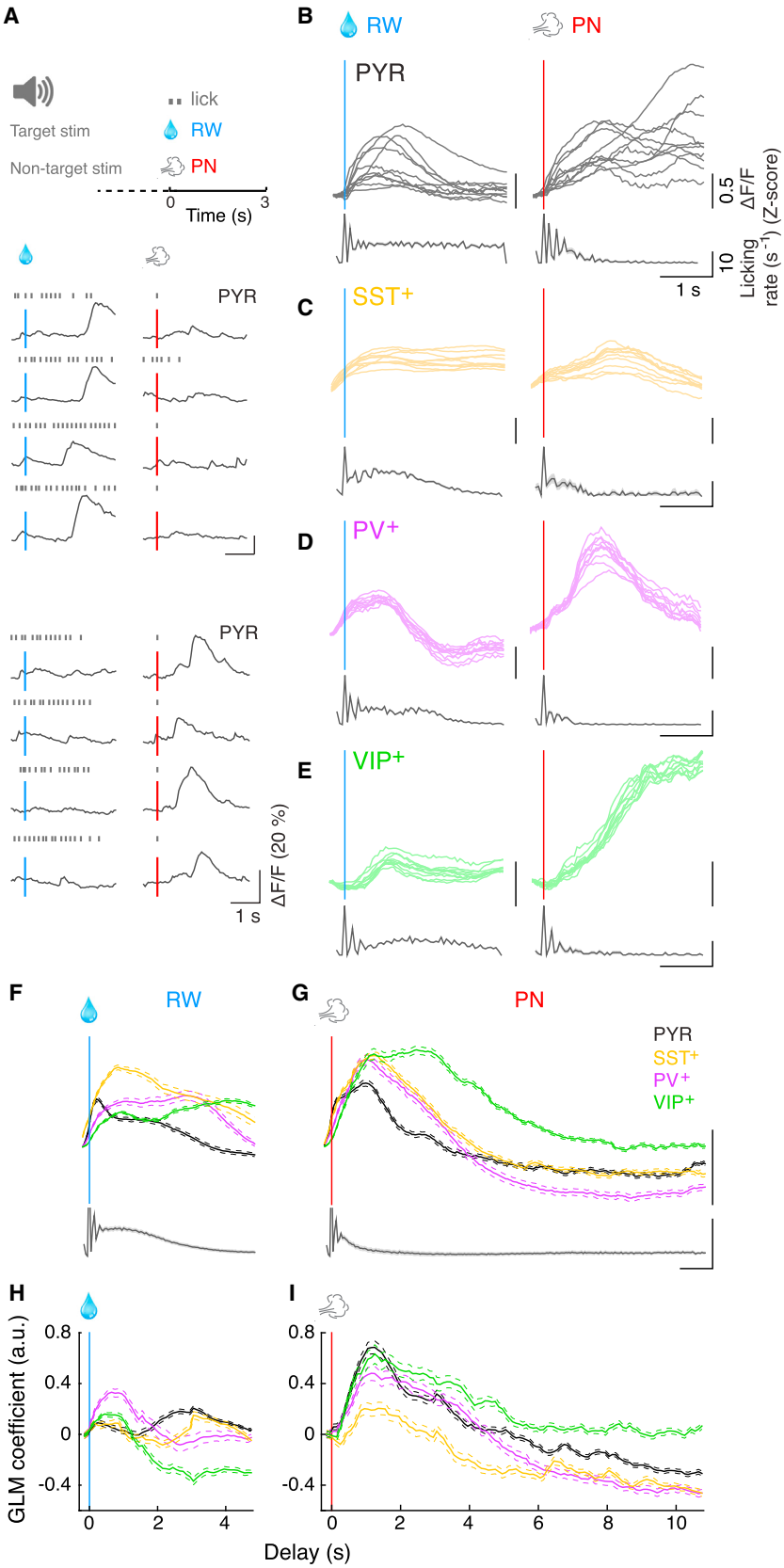

Figure 5. Outcome-Related Activity

(A) Top: schematic showing reward (RW, water drop) and punishment (PN, airpuff + time-out) as trial outcomes. Middle and bottom: ΔF/F traces of two PYR neurons at several example RW (left) and PN (right) trials.

(B–E) Trial-averaged ΔF/F traces at RW (left) and PN (right) from a representative recording for each cell type. Each plot contains trial-averaged responses of 10 example neurons recorded simultaneously in the same field of view (top, thin colored lines), with corresponding licking rate histograms (bottom, histograms were truncated for the bin at t = 0 since there is always a lick in that bin given that in our task design RW and PN were triggered by licking). The same neurons are shown on the left and right plots.

(F and G) Top: population average of responses to RW (F) and PN (G) averaged across all significantly modulated cells of each type. Bottom: population average of licking histograms. Thick lines, mean; thin dashed lines, ±SEM.

(H and I) GLM coefficients for RW (H) and PN (I) averaged across each cell type. Thick lines, mean; thin dashed lines, ±SEM.

See also Figure S4.

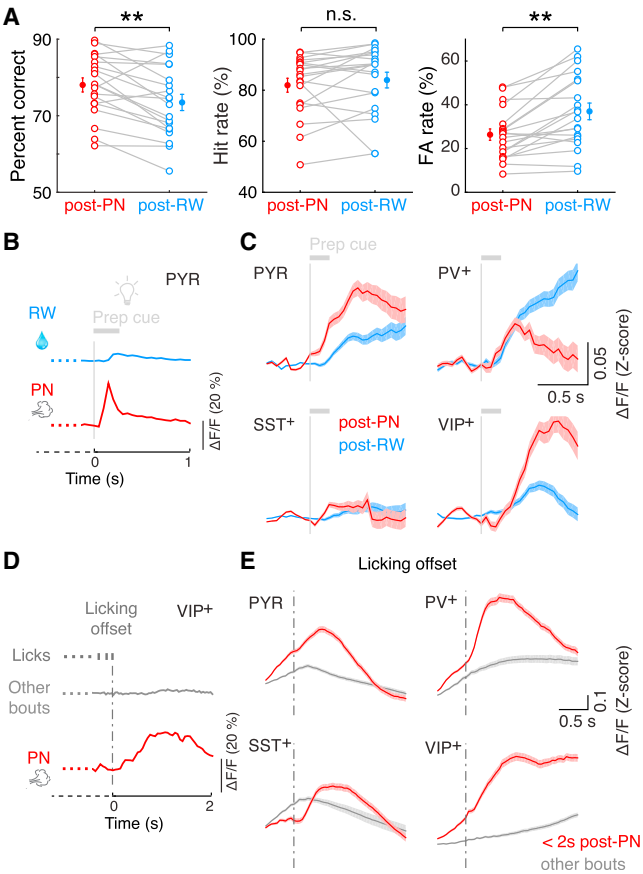

Figure 6. Modulation of Responses by Trial Outcome

(A) Behavioral adjustment based on previous outcome. Performance (% correct, left) was significantly higher, and false alarm (FA) rate (right) was significantly lower, in trials following punishment (post-PN) than those following reward (post-RW). Hit rates were not significantly different (middle). Lines correspond to individual mice (n = 20, from all genotypes). **p < 0.01, n.s., not significant. Closed circles and error bars, mean ± SEM.

(B) Responses of an example PYR neuron to prep cue in a post-RW trial (top, blue) and a post-PN trial (bottom, red).

(C) Responses to prep cue averaged across all task-modulated neurons of each cell type, in post-RW (blue) and post-PN (red) trials. PYR and VIP$^+$ neurons showed significantly higher responses in post-PN than post-RW trials, while PV$^+$ neurons showed the opposite difference. No significant difference was observed for SST$^+$ neurons. Shaded areas, ±SEM.

(D) Activity of an example VIP$^+$ neuron at lick-bout offset immediately following punishment (bottom, red) and from a lick bout occurring elsewhere in the trial (top, gray).

(E) Activity at licking offset averaged across all task-modulated neurons of each cell type. For all types, licking offset occurring <2 s after PN (red) was associated with higher activity than for other licking bouts (gray). Note that the licking offset responses in this analysis are based on the same data shown in Figure 4 except that we separated the lick bouts occurring after PN delivery and all other bouts. Shaded areas, ±SEM. Note that in some trials the airpuff triggered by a single lick inhibited further licking, so that licking offset coincided with PN. These trials were excluded in this analysis to minimize the confound between the activity evoked by PN and that associated with licking offset.

See also Figure S5.

300 μm, interneurons of the same subtype were highly correlated with each other, while PYR neurons showed much lower correlation (Figure 7A; $p < 10^{-20}$, $F_{3,18413} = 201.9$, one-way ANOVA, $p < 0.001$ for comparison between PYR and each interneuron subtype, Tukey's post hoc test), consistent with the impression based on visual inspection of the raw traces and event-triggered average of the recorded Ca^{2+} signals (Figures 1G–1J, 3B–3I, 4B–4E, and 5B–5E).

Note that the Ca^{2+} signals measured at the soma of each neuron were likely contaminated by out-of-focus neuropil fluorescence, and such contamination could affect the correlation between neurons. However, the higher correlation between interneurons than between pyramidal neurons was unlikely caused by the contamination, since neuropil fluorescence was subtracted from the measured somatic signals, and our finding was robust over a wide range of subtraction levels (see Supplemental Experimental Procedures). To further exclude the possibility that interneurons were less well focused than pyramidal cells and thus their signals were more contaminated by neuropil activity, we compared the pixel-wise activity map that was used to identify the regions of interest (ROIs) corresponding to cell bodies (Figure S1B, see Supplemental Experimental Procedures). We found that across cell types the ROIs were equally distinct from the surrounding neuropil regions (Figures S6A and S6B), indicating that interneurons were not less well focused. Moreover, when we repeated the analysis using only the neurons with highly distinct ROIs, the CCs were still much higher for interneurons than pyramidal neurons (Figure S6C). Thus, the higher CCs among interneurons were very unlikely caused by contamination from out-of-focus neuropil signals.

Since the CC between the fluorescence traces reflects not only the similarity in neuronal response properties but also correlated noise in their spiking activity (Cohen and Kohn, 2011), we next assessed the functional similarity between each pair of neurons by comparing their GLM coefficients (Figure 7B). The CCs between GLM coefficients were significantly lower for PYR neurons than each interneuron subtype (Figure 7C, $p < 10^{-20}$, $F_{3,16577} = 783.1$, one-way ANOVA, $p < 10^{-5}$ for comparison between PYR and each interneuron subtype, Tukey's post hoc test), indicating their greater functional heterogeneity.

Such functional heterogeneity is not surprising, as the PYR neuron population also consists of multiple subtypes. For example, PYR neurons in different cortical layers express distinct molecular markers and exhibit different synaptic connectivity (Douglas and Martin, 2004; Harris and Mrsic-Flogel, 2013). When we plotted the CC (between fluorescence traces or between GLM coefficients) as a function of the distance between PYR neurons either parallel or perpendicular to the dmPFC surface, we found that the CC decreased significantly more with perpendicular than with parallel distance (Figures 8A and 8B; $p_{axis} = 0.03$, $F_{axis(1,15428)} = 4.9$, $p_{distance} = 2.6 \times 10^{-19}$, $F_{distance(9,15428)} = 12.1$, $p_{interaction} = 0.002$, $F_{interaction(9,15428)} = 2.9$, two-way ANOVA with factors distance and axis). This anisotropy, which was not observed for the inhibitory neurons (Figure S7, $p_{interaction} > 0.3$ for all subtypes, two-way ANOVA), suggests that the activity patterns and response properties of PYR neurons varied much more across than within layers. In particular, we found that the response to prep cue changed

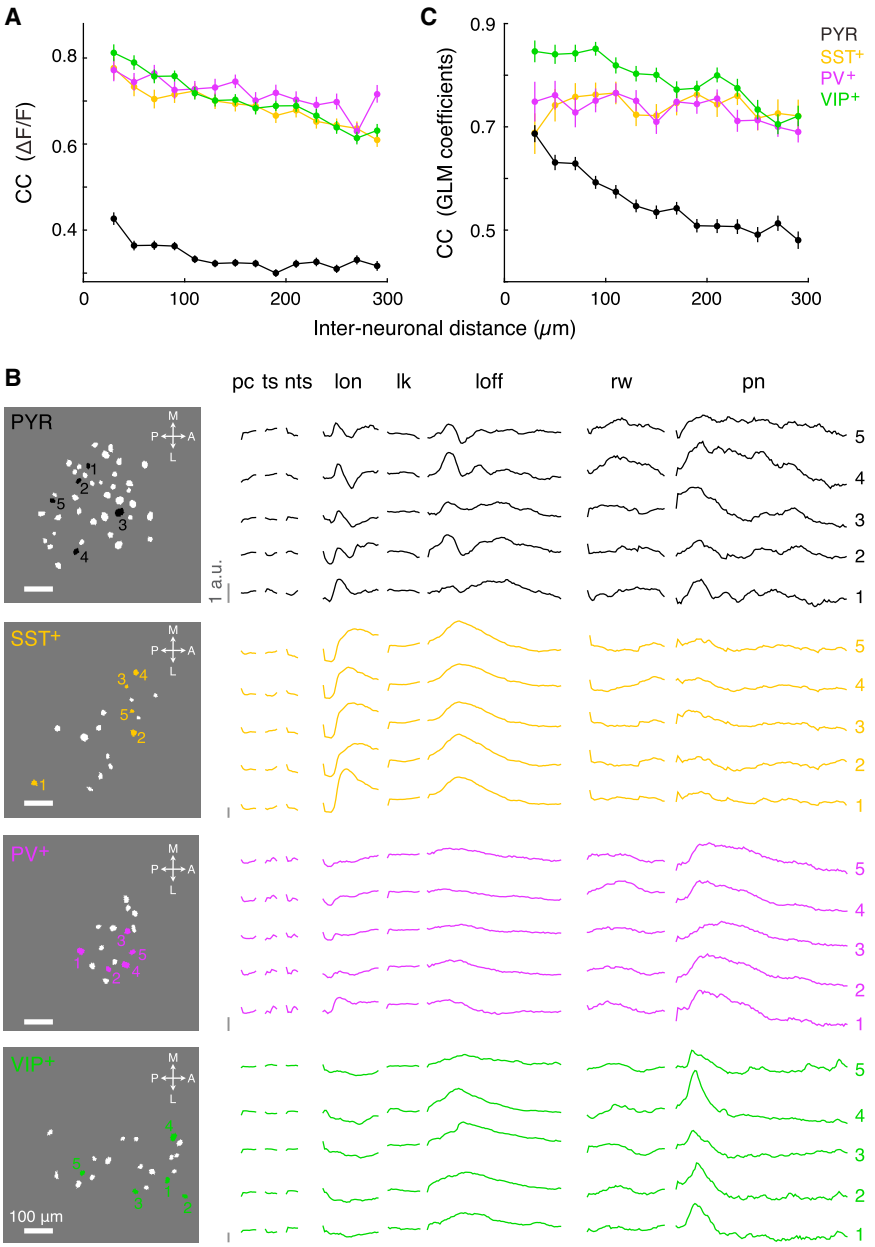

Figure 7. Spatial Organization of Task-Related Activity of Each Cell Type

(A) CC between ΔF/F traces of each cell pair versus distance of the pair, averaged across all recordings for each cell type (PYR: n = 9,500 neuron pairs; PV^+: n = 1,579; SST^+: n = 2,959; VIP^+: n = 4,379). Error bars, ±SEM.

(B) Example maps showing simultaneously imaged neurons in the same field of view (left, white and color). GLM coefficients of the neurons highlighted with color and indicated by numbers are plotted on the right. Note that inhibitory neurons of the same subtype showed similar GLM coefficients regardless of spatial position, whereas PYR cells are much more diverse. Pc, Prep cue; ts, target stimulus; nts, non-target stimulus; lon, licking onset; lk, mid-burst licks; loff, licking offset; rw, reward; pn, punishment.

(C) CC between GLM coefficients of each cell pair versus distance of the pair, averaged across all recordings for each cell type (PYR: n = 8,263 neuron pairs with significant GLM fits; PV^+: n = 1,562; SST^+: n = 2,865; VIP^+: n = 3,891). Error bars, ±SEM.

See also Figure S6.

systematically with laminar position, showing higher amplitude in superficial than deep layers. This was apparent both among simultaneously imaged neurons within the same field of view (Figure 8C) and among the entire PYR neuron population after combining all the imaging sessions from multiple mice (Figure 8D, $p = 1.5 \times 10^{-26}$, $F_{11,803} = 14.9$, one-way ANOVA). Thus, the preparatory signal that engages the PFC circuit for cognitive control appears to be stronger in superficial than deep layers of the dmPFC.

DISCUSSION

Using a simple goal-directed, go/no-go task, we have observed PFC neuron activity related to sensory, motor, and outcome components of the task, consistent with the notion of multiplexed encoding (Hyman et al., 2013; Machens et al., 2010; Mante et al., 2013; Rigotti et al., 2013). However, instead of randomly mixed selectivity for all neurons, we found clear differences across cell types, especially among inhibitory interneurons. Most task-related SST^+ neuron activity was associated with licking, whereas VIP^+ neuron activity was strongly modulated by action outcome. PV^+ neurons were the least selective, and they were the only class with robust responses to the auditory stimuli. PYR neurons formed a more heterogeneous population, and their functional properties varied across layers.

The various task-related activity we observed using microendoscopic imaging is consistent with many previous reports based on electrophysiology in the rodent PFC, including sensory-related activity (Euston et al., 2012; Insel and Barnes, 2014; Takehara-Nishiuchi and McNaughton, 2008), outcome-related activity (Burgos-Robles et al., 2013; Euston et al., 2012; Hyman et al., 2013; Insel and Barnes, 2014), and motor-related activity (Euston et al., 2012; Horst and Laubach, 2013; Hyman et al., 2013; Insel and Barnes, 2014; Jung et al., 1998). Thus, the lesion associated with our imaging experiment is unlikely to have caused global changes in the response properties of PFC neurons. The predominance of neuronal activity associated with licking is consistent with the notion that a primary function of the rodent dmPFC is action selection (Euston et al., 2012; Heidbreder and Groenewegen, 2003; Hyman et al., 2013), although it is also possible

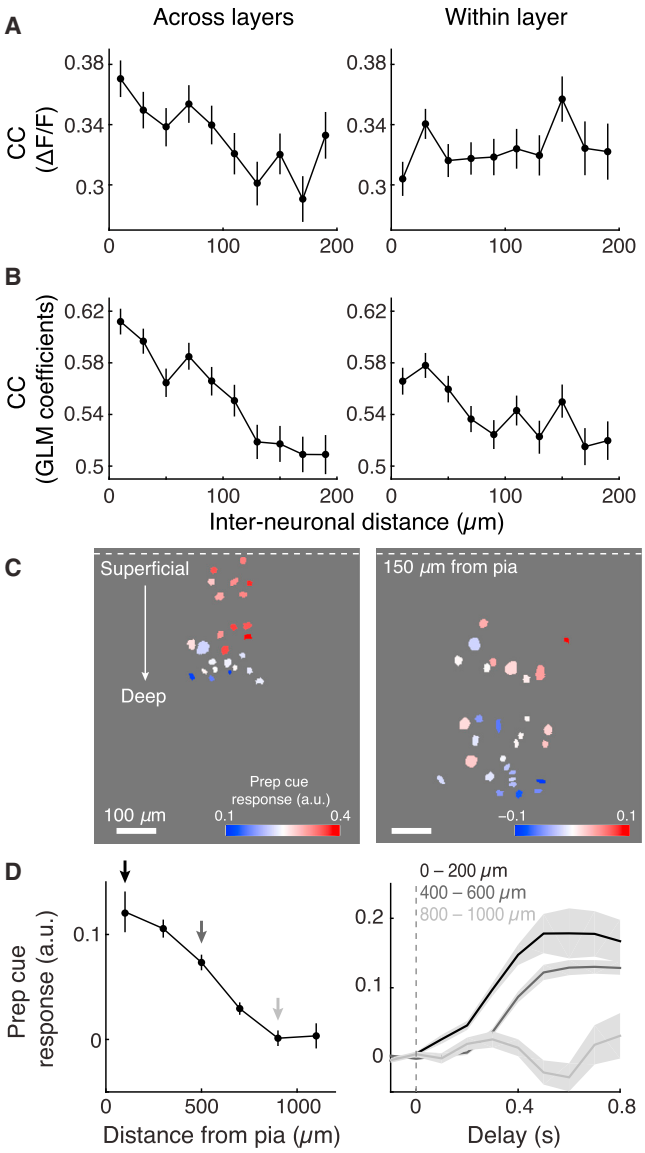

Figure 8. Laminar Organization of PYR Neuron Responses

(A) CC between ΔF/F traces of each PYR neuron pair versus distance across (perpendicular to) layers (left) or distance within (parallel to) each layer (right) (perpendicular: r = –0.77, p = 0.009, n = 8,547 pairs; parallel: r = 0.33, p = 0.34, n = 9,262 pairs). Error bars, ±SEM.

(B) CC between GLM coefficients of each PYR neuron pair versus distance across (perpendicular to) layers (left) or distance within (parallel to) each layer (right) (perpendicular: r = –0.96, p = 1.1×10^{-5}, n = 7,425 pairs with significant GLM fits; parallel: –0.79, p = 0.007, n = 8,023 pairs). Error bars, ±SEM.

(C) Two example maps (from different animals) showing the spatial distribution of prep cue response amplitude (color-coded, scale bar at bottom). Note that in both examples the responses were larger in more superficial cells.

(D) Left: population average of prep cue responses (n = 816) as a function of estimated distance from the pia. Right: average prep cue GLM coefficients at three cortical depths (indicated by arrows on the left). Shaded areas, ±SEM. See also Figure S7.

that, instead of driving behavior, the activity reflects efference copy of the motor command or movement-induced neuromodulation, as has been observed in sensory cortical areas (Fu et al., 2014; Lee et al., 2014a; Polack et al., 2013; Schneider et al., 2014). Among all the cell types studied, SST$^+$ neurons showed the strongest activity at licking onset (Figures 4F and 4H). Since these interneurons target dendrites, they can provide potent inhibition that effectively suppresses synaptic inputs to pyramidal neurons over a large cortical region (Adesnik et al., 2012; Lovett-Barron et al., 2014; Silberberg and Markram, 2007; Zhang et al., 2014). Thus, their increased activity at licking onset may serve to suppress distracting inputs to the PFC once the decision to lick has been made (Wang et al., 2004).

The robust, long-lasting responses of dmPFC neurons to PN (Figures 5G and 5I) may originate from neuromodulatory inputs, such as the dopaminergic projection from the midbrain (Lammel et al., 2012) and the cholinergic input from the basal forebrain (Letzkus et al., 2011; Pinto et al., 2013; Poorthuis et al., 2014). VIP$^+$ neurons, which were particularly susceptible to PN modulation, have been shown to be strongly activated by basal forebrain input through nicotinic acetylcholine receptors (Alitto and Dan, 2012; Porter et al., 1999). A previous study showed that VIP$^+$ neurons in the auditory cortex also respond to punishment (Pi et al., 2013), suggesting that the signal activated by PN is widely broadcast to multiple cortical areas. Such long-range modulatory inputs may act through local VIP$^+$ neurons to regulate cortical computation. For example, the enhanced responses of VIP$^+$ and PYR neurons to the prep cue in post-PN trials (Figure 6C) could be caused by neuromodulatory inputs that activate VIP$^+$ neurons, which in turn disinhibit PYR neurons (Fu et al., 2014; Lee et al., 2013; Pi et al., 2013; Poorthuis et al., 2014; Wang et al., 2004; Zhang et al., 2014).

In addition to licking and trial outcome, PV$^+$ neurons also responded to the auditory stimuli (Figures 3H and 3K), consistent with a recent report on fast-spiking cells in the rat mPFC (Insel and Barnes, 2014). The wide-ranging responses of PV$^+$ neurons are reminiscent of their broad tuning in sensory cortex (Hofer et al., 2011; Kerlin et al., 2010), likely caused by non-selective innervation from nearby PYR neurons (Bock et al., 2011; Packer and Yuste, 2011) and serving to sharpen the selectivity of PYR neurons (Hamilton et al., 2013; Lee et al., 2012). Surprisingly, responses to the auditory stimuli were rarely observed in PYR neurons (Figures 3F and S2A), which is consistent with a recent study in rat mPFC (Insel and Barnes, 2014) but contrary to previous observations of sensory responses in many PFC neurons (Euston et al., 2012; Miller and Cohen, 2001). One possibility is that these responses reflect the attention-grabbing properties of the cues rather than representing the sensory information per se (Fuster, 2008). In the present study, trial start was signaled by the light flash 1 s before the auditory stimulus, which may be why more neurons responded to the visual prep cue than to the auditory stimulus.

A previous study in the monkey PFC showed that fast-spiking neurons are highly correlated with each other (Constantinidis and Goldman-Rakic, 2002). We have found that in addition to the fast-spiking PV$^+$ neurons, other interneurons of the same subtype were also much more correlated than PYR cells, perhaps partly due to the extensive gap junction coupling within each subtype (Galarreta and Hestrin, 1999; Gibson et al., 1999; but see Kvitsiani et al., 2013).

In contrast to inhibitory interneurons, pyramidal neuron responses were highly diverse, consistent with previous reports in the PFC (Euston et al., 2012; Hyman et al., 2013; Kvitsiani et al., 2013; Miller and Cohen, 2001; Narayanan and Laubach, 2006; Rigotti et al., 2013). This diversity, however, was not distributed randomly. The laminar differences in PYR neuron response properties are likely related to layer-specific synaptic connectivity (Gabbott et al., 2005). In particular, the larger responses to the prep cue found in superficial neurons (Figures 8C and 8D) could be due to the preferential targeting of superficial layers by the axonal projections from visual cortical areas (Van Eden et al., 1992). Of course, the functional diversity of PYR neurons cannot be accounted for by their laminar differences alone. The response properties are also likely to be organized according to their developmental lineage (Li et al., 2012; Ohtsuki et al., 2012) and projection targets (Chen et al., 2013a; Glickfeld et al., 2013; Jarosiewicz et al., 2012; Yamashita et al., 2013).

Recent optogenetic studies have demonstrated the causal roles of long-range projections from the PFC in controlling multiple types of behavior (Challis et al., 2014; Lee et al., 2014b; Warden et al., 2012; Zhang et al., 2014). An equally important question is how different neurons within the PFC microcircuit are activated by various task-related events. By characterizing the functional properties of PFC neurons of different subtypes and laminar locations, our study complements optogenetic manipulations to reveal how the PFC coordinates perception, action, and adaptive control to optimize goal-directed behavior.

EXPERIMENTAL PROCEDURES

Animals and Surgery

All procedures were approved by the Animal Care and Use Committee at the University of California, Berkeley. Experiments were performed on adult CaMKIIα-, PV-, SST-, and VIP-Cre mice (2–5 months old, 20–35 g, both male and female).

Animals used in imaging experiments underwent two surgical procedures. In the first surgery we implanted a stainless steel headplate for head fixation and injected AAV encoding GCaMP6f (Chen et al., 2013b). After a week of recovery, the mouse underwent the initial stages of behavioral training for ~2 weeks (see below). We then interrupted water restriction and performed a second surgery to implant the gradient refractive index (GRIN) lens (Inscopix; diameter: 1 mm; length: 4.2 mm; pitch: 0.5; numerical aperture: 0.5). After a recovery period of at least 3 days, water restriction was reinstated and behavioral training resumed.

Detailed information on the surgical procedures and mouse lines can be found in the Supplemental Experimental Procedures.

Histology and Immunohistochemistry

We performed histology to confirm the location of the implanted GRIN lens or optic fiber, and immunohistochemistry for CaMKIIα, PV, SST, and VIP to confirm cell-type specificity and efficiency of GCaMP6f expression. Details can be found in the Supplemental Experimental Procedures.

Behavior

We trained head-fixed mice on a go/no-go auditory task (Figure 1A). The tones were generated with MATLAB (MathWorks) and presented through standard computer speakers (Logitech) controlled by on-board sound cards. The speakers were calibrated to ensure that the target and non-target tones had the same intensity of 65 dB. Mice were water restricted and ordinarily had access to water only during training. However, additional water was given if necessary to ensure that their body weight (monitored daily) did not drop below 85% of the starting value.

After an initial ~7 days of habituation, response shaping, and conditioning—details on these procedures and the apparatus can be found elsewhere (Pinto et al., 2013)—the mice were moved to the auditory discrimination task. The start of each trial was signaled by a 200-ms light flash on an LCD screen placed 15 cm from the left eye. The auditory stimulus was presented 1 s after the onset of the flash with a maximum duration of 2 s. Licking during the first 500 ms of stimulus presentation had no consequence, and this grace period was followed by a 1.5 s response window indicated by lighting of the screen. Licking during the response window of a go trial (presentation of the target stimulus) was counted as a *hit*, while no licking was counted as a *miss*. In no-go trials (non-target stimulus), licking was counted as a *false alarm* and no licking as a *correct rejection*. The first lick during the response window interrupted the auditory stimulus and triggered either reward or punishment: in go trials, licking triggered a water reward (~4 μl), and in no-go trials licking triggered an airpuff to the cheek (15–20 psi, 200 ms) and an 8 s time-out period. The inter-trial interval was 3 s, with an extra 2 s for reward consumption after hit trials. Mice were trained daily (except for a ~4-day break for GRIN lens implantation, see above) until reaching criterion performance, defined as >70% correct trials for at least 3 consecutive days or >75% correct for 2 consecutive days. These criteria were chosen to avoid overtraining prior to the experimental manipulations, while ensuring above-chance performance. Once the mice reached these criteria, we started performing pharmacological inactivation or Ca^{2+} imaging experiments. No additional shaping procedures were required after the surgery for GRIN lens implantation, since there was no noticeable drop in performance caused by the procedure.

Inactivation Experiments

For pharmacological inactivation experiments, we injected 0.375 μl of either the $GABA_A$ agonist muscimol (Sigma, 1 μg/μl) or saline at a rate of 0.25 μl/min, bilaterally. We waited for 5 min at the end of the injection to allow diffusion of the drug before removing the cannula. Behavioral experiments started 30 min after the injections. Further details on these experiments can be found in the Supplemental Experimental Procedures.

Microendoscopic Ca^{2+} Imaging

We performed cellular-resolution microendoscopic Ca^{2+} imaging from genetically defined cell types in the right dmPFC using a miniaturized integrated fluorescence microscope (Inscopix; 20× objective; LED power: 0.2–0.7 mW; CMOS sensor resolution: 1,440 × 1,080 pixels) coupled to a GRIN lens (Ghosh et al., 2011) (Figure 1D).

Images were acquired at 20 frames per second using nVista HD (Inscopix) running on a dedicated PC. At the beginning of each imaging session, we removed the protective cap from the previously implanted baseplate and attached the microscope. The imaging field of view (maximal size, ~600 × 800 μm) was then selected by adjusting the focus and selecting a sub-region containing clearly identifiable cells. Focal planes were 50–200 μm below the bottom of the lens. To avoid repeated imaging from the same neurons, we systematically changed the focal plane for different imaging sessions. Behavioral events were synchronized with imaging by acquiring analog voltage signals output by both the imaging acquisition and behavioral control software using custom code written in LabVIEW (National Instruments) running on a third PC. Details on inclusion criteria for imaging sessions can be found in the Supplemental Experimental Procedures.

Image Processing

The acquired images were first spatially downsampled by a factor of 4 using nVista Viewer (Inscopix). Image stacks were then corrected for lateral motion, and regions of interest (ROIs) were selected on a pixel-wise activity map (Figure S1B). Average fluorescence was extracted for each ROI and corrected for potential neuropil contamination ($F_{corrected}$). ΔF/F was calculated as $\Delta F/F(t) = (F_{corrected}(t) - < F >)/< F >$, where $< F >$ is the average fluorescence across the entire recording, because there were no true "baseline periods" during the behavioral task. Unless otherwise stated, ΔF/F traces are *Z* scored. Details on image processing procedures can be found in the Supplemental Experimental Procedures.

Data Analysis

For behavioral data analysis, *hit rate* was defined as # *hits* / (# *hits* + # *misses*) and *false alarm rate* as # *false alarms* / (# *false alarms* + # *correct rejections*). Behavioral performance was measured by *percent correct* = (# *hits* + # *correct rejections*) / # trials. Individual behavioral sessions were truncated for analysis at the last trial in which the mouse licked. To analyze the effects of PFC inactivation (Figures 1C and S1A) and the outcome dependence of behavioral performance (Figure 6A), we concatenated individual sessions to obtain a single performance value for each animal.

To assess whether a neuron was significantly modulated by the task, we performed a three-way ANOVA with factors stimulus identity (target versus non-target), action (lick versus no lick) and epoch [preparation (0.5 s following start cue), stimulus (0.5 s following the onset of auditory stimulus presentation), early outcome (1 s following water or airpuff delivery), and late outcome (1–3 s after delivery)]. A neuron was deemed significantly modulated if $p < 0.01$ for at least one of the factors or interaction terms.

We used a generalized linear model (GLM) to quantify task-related activity of the cells, regressing the recorded Ca^{2+} signals against a time series of task events (Miri et al., 2011). Models were fit using ridge regression. For statistical comparisons between cell types, we computed the mean GLM coefficient for each regressor over a given time period (PN: 0–4 s; RW: 0–2 s; stimulus: 0–0.2 s; prep cue: 0–0.8 s; licking onset: −0.5–3 s; licking offset: −0.5–8 s) after baseline subtraction. Only neurons that were significantly modulated by the task with significant GLM fits were included in the comparison.

Note that although the amplitude of ΔF/F corresponding to a single spike differs across cell type (Chen et al., 2013b), the response properties quantified by GLM are insensitive to the difference as long as the relationship between ΔF/F and firing rate is linear. For GCaMP6f, the linearity has been shown for PYR and PV^+ cells (Chen et al., 2013b). A previous study using Oregon green BAPTA also showed a linear relationship for SST^+ cells (Kwan and Dan, 2012).

Further details on data analysis and the GLM fitting procedure can be found in the Supplemental Experimental Procedures.

General Statistics

Datasets were tested for normality using the Lilliefors modification of the Kolmogorov-Smirnov test and then compared using appropriate tests (t or rank tests, all two sided unless stated otherwise). Groups being compared had similar variance. Statistical significance of experiments with factorial design was assessed using ANOVAs followed by Tukey's post hoc test with correction for multiple comparisons. Unless otherwise stated, data are presented as mean ± SEM.

SUPPLEMENTAL INFORMATION

Supplemental Information includes Supplemental Experimental Procedures, seven figures, and one movie and can be found with this article online at http://dx.doi.org/10.1016/j.neuron.2015.06.021.

AUTHOR CONTRIBUTIONS

L.P. performed the experiments and analyzed the data. L.P. and Y.D. conceived and designed the experiments and wrote the paper.

ACKNOWLEDGMENTS

We thank D.E. Feldman, C.D. Brody, J.D. Wallis, C.C. Rodgers, J.M. Cox, T.C. Harrison, Y. Li, and M.J. Goard for helpful discussions and M. Zhang, Y. Ziv, M. Schnitzer, L. Burns, E. Cocker, C.C. Rodgers, J. Tang, and C. Elder for technical assistance. GCaMP6f was provided by V. Jayaraman, R.A. Kerr, D.S. Kim, L.L. Looger, and K. Svoboda from the GENIE Project. This work was supported by a Ruth L. Kirschstein National Research Service Award F31NS084696 from NINDS (L.P.).

Received: April 5, 2015
Revised: May 5, 2015
Accepted: June 16, 2015
Published: July 2, 2015

REFERENCES

Adesnik, H., Bruns, W., Taniguchi, H., Huang, Z.J., and Scanziani, M. (2012). A neural circuit for spatial summation in visual cortex. Nature *490*, 226–231.

Alitto, H.J., and Dan, Y. (2012). Cell-type-specific modulation of neocortical activity by basal forebrain input. Front. Syst. Neurosci. *6*, 79.

Bissonette, G.B., Martins, G.J., Franz, T.M., Harper, E.S., Schoenbaum, G., and Powell, E.M. (2008). Double dissociation of the effects of medial and orbital prefrontal cortical lesions on attentional and affective shifts in mice. J. Neurosci. *28*, 11124–11130.

Bock, D.D., Lee, W.-C.A., Kerlin, A.M., Andermann, M.L., Hood, G., Wetzel, A.W., Yurgenson, S., Soucy, E.R., Kim, H.S., and Reid, R.C. (2011). Network anatomy and in vivo physiology of visual cortical neurons. Nature *471*, 177–182.

Burgos-Robles, A., Bravo-Rivera, H., and Quirk, G.J. (2013). Prelimbic and infralimbic neurons signal distinct aspects of appetitive instrumental behavior. PLoS ONE *8*, e57575.

Challis, C., Beck, S.G., and Berton, O. (2014). Optogenetic modulation of descending prefrontocortical inputs to the dorsal raphe bidirectionally bias socioaffective choices after social defeat. Front. Behav. Neurosci. *8*, 43.

Chen, J.L., Carta, S., Soldado-Magraner, J., Schneider, B.L., and Helmchen, F. (2013a). Behaviour-dependent recruitment of long-range projection neurons in somatosensory cortex. Nature *499*, 336–340.

Chen, T.-W., Wardill, T.J., Sun, Y., Pulver, S.R., Renninger, S.L., Baohan, A., Schreiter, E.R., Kerr, R.A., Orger, M.B., Jayaraman, V., et al. (2013b). Ultrasensitive fluorescent proteins for imaging neuronal activity. Nature *499*, 295–300.

Cohen, M.R., and Kohn, A. (2011). Measuring and interpreting neuronal correlations. Nat. Neurosci. *14*, 811–819.

Constantinidis, C., and Goldman-Rakic, P.S. (2002). Correlated discharges among putative pyramidal neurons and interneurons in the primate prefrontal cortex. J. Neurophysiol. *88*, 3487–3497.

Courtin, J., Chaudun, F., Rozeske, R.R., Karalis, N., Gonzalez-Campo, C., Wurtz, H., Abdi, A., Baufreton, J., Bienvenu, T.C.M., and Herry, C. (2014). Prefrontal parvalbumin interneurons shape neuronal activity to drive fear expression. Nature *505*, 92–96.

Desimone, R., and Duncan, J. (1995). Neural mechanisms of selective visual attention. Annu. Rev. Neurosci. *18*, 193–222.

Douglas, R.J., and Martin, K.A.C. (2004). Neuronal circuits of the neocortex. Annu. Rev. Neurosci. *27*, 419–451.

Euston, D.R., Gruber, A.J., and McNaughton, B.L. (2012). The role of medial prefrontal cortex in memory and decision making. Neuron *76*, 1057–1070.

Fu, Y., Tucciarone, J.M., Espinosa, J.S., Sheng, N., Darcy, D.P., Nicoll, R.A., Huang, Z.J., and Stryker, M.P. (2014). A cortical circuit for gain control by behavioral state. Cell *156*, 1139–1152.

Fujii, N., and Graybiel, A.M. (2003). Representation of action sequence boundaries by macaque prefrontal cortical neurons. Science *301*, 1246–1249.

Fuster, J. (2008). The Prefrontal Cortex (London: Academic Press).

Gabbott, P.L.A., Warner, T.A., Jays, P.R.L., Salway, P., and Busby, S.J. (2005). Prefrontal cortex in the rat: projections to subcortical autonomic, motor, and limbic centers. J. Comp. Neurol. *492*, 145–177.

Galarreta, M., and Hestrin, S. (1999). A network of fast-spiking cells in the neocortex connected by electrical synapses. Nature *402*, 72–75.

Gentet, L.J., Kremer, Y., Taniguchi, H., Huang, Z.J., Staiger, J.F., and Petersen, C.C.H. (2012). Unique functional properties of somatostatin-expressing GABAergic neurons in mouse barrel cortex. Nat. Neurosci. *15*, 607–612.

Ghosh, K.K., Burns, L.D., Cocker, E.D., Nimmerjahn, A., Ziv, Y., Gamal, A.E., and Schnitzer, M.J. (2011). Miniaturized integration of a fluorescence microscope. Nat. Methods *8*, 871–878.

Gibson, J.R., Beierlein, M., and Connors, B.W. (1999). Two networks of electrically coupled inhibitory neurons in neocortex. Nature *402*, 75–79.

Glickfeld, L.L., Andermann, M.L., Bonin, V., and Reid, R.C. (2013). Cortico-cortical projections in mouse visual cortex are functionally target specific. Nat. Neurosci. *16*, 219–226.

Hamilton, L.S., Sohl-Dickstein, J., Huth, A.G., Carels, V.M., Deisseroth, K., and Bao, S. (2013). Optogenetic activation of an inhibitory network enhances feedforward functional connectivity in auditory cortex. Neuron *80*, 1066–1076.

Hanks, T.D., Kopec, C.D., Brunton, B.W., Duan, C.A., Erlich, J.C., and Brody, C.D. (2015). Distinct relationships of parietal and prefrontal cortices to evidence accumulation. Nature *520*, 220–223.

Harris, K.D., and Mrsic-Flogel, T.D. (2013). Cortical connectivity and sensory coding. Nature *503*, 51–58.

Hayden, B.Y., Nair, A.C., McCoy, A.N., and Platt, M.L. (2008). Posterior cingulate cortex mediates outcome-contingent allocation of behavior. Neuron *60*, 19–25.

Heidbreder, C.A., and Groenewegen, H.J. (2003). The medial prefrontal cortex in the rat: evidence for a dorso-ventral distinction based upon functional and anatomical characteristics. Neurosci. Biobehav. Rev. *27*, 555–579.

Hofer, S.B., Ko, H., Pichler, B., Vogelstein, J., Roš, H., Zeng, H., Lein, E., Lesica, N.A., and Mrsic-Flogel, T.D. (2011). Differential connectivity and response dynamics of excitatory and inhibitory neurons in visual cortex. Nat. Neurosci. *14*, 1045–1052.

Horst, N.K., and Laubach, M. (2013). Reward-related activity in the medial prefrontal cortex is driven by consumption. Front. Neurosci. *7*, 56.

Hyman, J.M., Whitman, J., Emberly, E., Woodward, T.S., and Seamans, J.K. (2013). Action and outcome activity state patterns in the anterior cingulate cortex. Cereb. Cortex *23*, 1257–1268.

Insel, N., and Barnes, C.A. (2014). Differential activation of fast-spiking and regular-firing neuron populations during movement and reward in the dorsal medial frontal cortex. Cereb. Cortex. Published online April 3, 2014. http://dx.doi.org/10.1093/cercor/bhu062.

Ito, S., Stuphorn, V., Brown, J.W., and Schall, J.D. (2003). Performance monitoring by the anterior cingulate cortex during saccade countermanding. Science *302*, 120–122.

Jarosiewicz, B., Schummers, J., Malik, W.Q., Brown, E.N., and Sur, M. (2012). Functional biases in visual cortex neurons with identified projections to higher cortical targets. Curr. Biol. *22*, 269–277.

Jung, M.W., Qin, Y., McNaughton, B.L., and Barnes, C.A. (1998). Firing characteristics of deep layer neurons in prefrontal cortex in rats performing spatial working memory tasks. Cereb. Cortex *8*, 437–450.

Kerlin, A.M., Andermann, M.L., Berezovskii, V.K., and Reid, R.C. (2010). Broadly tuned response properties of diverse inhibitory neuron subtypes in mouse visual cortex. Neuron *67*, 858–871.

Kvitsiani, D., Ranade, S., Hangya, B., Taniguchi, H., Huang, J.Z., and Kepecs, A. (2013). Distinct behavioural and network correlates of two interneuron types in prefrontal cortex. Nature *498*, 363–366.

Kwan, A.C., and Dan, Y. (2012). Dissection of cortical microcircuits by single-neuron stimulation in vivo. Curr. Biol. *22*, 1459–1467.

Lammel, S., Lim, B.K., Ran, C., Huang, K.W., Betley, M.J., Tye, K.M., Deisseroth, K., and Malenka, R.C. (2012). Input-specific control of reward and aversion in the ventral tegmental area. Nature *491*, 212–217.

Lee, S.-H., Kwan, A.C., Zhang, S., Phoumthipphavong, V., Flannery, J.G., Masmanidis, S.C., Taniguchi, H., Huang, Z.J., Zhang, F., Boyden, E.S., et al. (2012). Activation of specific interneurons improves V1 feature selectivity and visual perception. Nature *488*, 379–383.

Lee, S., Kruglikov, I., Huang, Z.J., Fishell, G., and Rudy, B. (2013). A disinhibitory circuit mediates motor integration in the somatosensory cortex. Nat. Neurosci. *16*, 1662–1670.

Lee, A.M., Hoy, J.L., Bonci, A., Wilbrecht, L., Stryker, M.P., and Niell, C.M. (2014a). Identification of a brainstem circuit regulating visual cortical state in parallel with locomotion. Neuron *83*, 455–466.

Lee, A.T., Vogt, D., Rubenstein, J.L., and Sohal, V.S. (2014b). A class of GABAergic neurons in the prefrontal cortex sends long-range projections to the nucleus accumbens and elicits acute avoidance behavior. J. Neurosci. *34*, 11519–11525.

Letzkus, J.J., Wolff, S.B.E., Meyer, E.M.M., Tovote, P., Courtin, J., Herry, C., and Lüthi, A. (2011). A disinhibitory microcircuit for associative fear learning in the auditory cortex. Nature *480*, 331–335.

Li, Y., Lu, H., Cheng, P.-L., Ge, S., Xu, H., Shi, S.-H., and Dan, Y. (2012). Clonally related visual cortical neurons show similar stimulus feature selectivity. Nature *486*, 118–121.

Lovett-Barron, M., Kaifosh, P., Kheirbek, M.A., Danielson, N., Zaremba, J.D., Reardon, T.R., Turi, G.F., Hen, R., Zemelman, B.V., and Losonczy, A. (2014). Dendritic inhibition in the hippocampus supports fear learning. Science *343*, 857–863.

Machens, C.K., Romo, R., and Brody, C.D. (2010). Functional, but not anatomical, separation of "what" and "when" in prefrontal cortex. J. Neurosci. *30*, 350–360.

Mante, V., Sussillo, D., Shenoy, K.V., and Newsome, W.T. (2013). Context-dependent computation by recurrent dynamics in prefrontal cortex. Nature *503*, 78–84.

Matsumoto, M., Matsumoto, K., Abe, H., and Tanaka, K. (2007). Medial prefrontal cell activity signaling prediction errors of action values. Nat. Neurosci. *10*, 647–656.

Miller, E.K., and Cohen, J.D. (2001). An integrative theory of prefrontal cortex function. Annu. Rev. Neurosci. *24*, 167–202.

Miri, A., Daie, K., Burdine, R.D., Aksay, E., and Tank, D.W. (2011). Regression-based identification of behavior-encoding neurons during large-scale optical imaging of neural activity at cellular resolution. J. Neurophysiol. *105*, 964–980.

Narayanan, N.S., and Laubach, M. (2006). Top-down control of motor cortex ensembles by dorsomedial prefrontal cortex. Neuron *52*, 921–931.

Narayanan, N.S., Cavanagh, J.F., Frank, M.J., and Laubach, M. (2013). Common medial frontal mechanisms of adaptive control in humans and rodents. Nat. Neurosci. *16*, 1888–1895.

Ohtsuki, G., Nishiyama, M., Yoshida, T., Murakami, T., Histed, M., Lois, C., and Ohki, K. (2012). Similarity of visual selectivity among clonally related neurons in visual cortex. Neuron *75*, 65–72.

Packer, A.M., and Yuste, R. (2011). Dense, unspecific connectivity of neocortical parvalbumin-positive interneurons: a canonical microcircuit for inhibition? J. Neurosci. *31*, 13260–13271.

Pi, H.-J., Hangya, B., Kvitsiani, D., Sanders, J.I., Huang, Z.J., and Kepecs, A. (2013). Cortical interneurons that specialize in disinhibitory control. Nature *503*, 521–524.

Pinto, L., Goard, M.J., Estandian, D., Xu, M., Kwan, A.C., Lee, S.-H., Harrison, T.C., Feng, G., and Dan, Y. (2013). Fast modulation of visual perception by basal forebrain cholinergic neurons. Nat. Neurosci. *16*, 1857–1863.

Polack, P.-O., Friedman, J., and Golshani, P. (2013). Cellular mechanisms of brain state-dependent gain modulation in visual cortex. Nat. Neurosci. *16*, 1331–1339.

Poorthuis, R.B., Enke, L., and Letzkus, J.J. (2014). Cholinergic circuit modulation through differential recruitment of neocortical interneuron types during behaviour. J. Physiol. *592*, 4155–4164.

Porter, J.T., Cauli, B., Tsuzuki, K., Lambolez, B., Rossier, J., and Audinat, E. (1999). Selective excitation of subtypes of neocortical interneurons by nicotinic receptors. J. Neurosci. *19*, 5228–5235.

Ridderinkhof, K.R., Ullsperger, M., Crone, E.A., and Nieuwenhuis, S. (2004). The role of the medial frontal cortex in cognitive control. Science *306*, 443–447.

Rigotti, M., Barak, O., Warden, M.R., Wang, X.-J., Daw, N.D., Miller, E.K., and Fusi, S. (2013). The importance of mixed selectivity in complex cognitive tasks. Nature *497*, 585–590.

Rudy, B., Fishell, G., Lee, S., and Hjerling-Leffler, J. (2011). Three groups of interneurons account for nearly 100% of neocortical GABAergic neurons. Dev. Neurobiol. *71*, 45–61.

Schall, J.D., Stuphorn, V., and Brown, J.W. (2002). Monitoring and control of action by the frontal lobes. Neuron *36*, 309–322.

Schneider, D.M., Nelson, A., and Mooney, R. (2014). A synaptic and circuit basis for corollary discharge in the auditory cortex. Nature *513*, 189–194.

Silberberg, G., and Markram, H. (2007). Disynaptic inhibition between neocortical pyramidal cells mediated by Martinotti cells. Neuron *53*, 735–746.

Sparta, D.R., Hovelsø, N., Mason, A.O., Kantak, P.A., Ung, R.L., Decot, H.K., and Stuber, G.D. (2014). Activation of prefrontal cortical parvalbumin interneurons facilitates extinction of reward-seeking behavior. J. Neurosci. *34*, 3699–3705.

Squire, R.F., Noudoost, B., Schafer, R.J., and Moore, T. (2013). Prefrontal contributions to visual selective attention. Annu. Rev. Neurosci. *36*, 451–466.

Takehara-Nishiuchi, K., and McNaughton, B.L. (2008). Spontaneous changes of neocortical code for associative memory during consolidation. Science *322*, 960–963.

Van Eden, C.G., Lamme, V.A.F., and Uylings, H.B.M. (1992). Heterotopic cortical afferents to the medial prefrontal cortex in the rat. A combined retrograde and anterograde tracer study. Eur. J. Neurosci. *4*, 77–97.

Wallis, J.D., and Kennerley, S.W. (2010). Heterogeneous reward signals in prefrontal cortex. Curr. Opin. Neurobiol. *20*, 191–198.

Wang, X.-J., Tegnér, J., Constantinidis, C., and Goldman-Rakic, P.S. (2004). Division of labor among distinct subtypes of inhibitory neurons in a cortical microcircuit of working memory. Proc. Natl. Acad. Sci. USA *101*, 1368–1373.

Warden, M.R., Selimbeyoglu, A., Mirzabekov, J.J., Lo, M., Thompson, K.R., Kim, S.-Y., Adhikari, A., Tye, K.M., Frank, L.M., and Deisseroth, K. (2012). A prefrontal cortex-brainstem neuronal projection that controls response to behavioural challenge. Nature *492*, 428–432.

Watanabe, M. (1996). Reward expectancy in primate prefrontal neurons. Nature *382*, 629–632.

Xu, X., Roby, K.D., and Callaway, E.M. (2010). Immunochemical characterization of inhibitory mouse cortical neurons: three chemically distinct classes of inhibitory cells. J. Comp. Neurol. *518*, 389–404.

Yamashita, T., Pala, A., Pedrido, L., Kremer, Y., Welker, E., and Petersen, C.C.H. (2013). Membrane potential dynamics of neocortical projection neurons driving target-specific signals. Neuron *80*, 1477–1490.

Zhang, S., Xu, M., Kamigaki, T., Hoang Do, J.P., Chang, W.C., Jenvay, S., Miyamichi, K., Luo, L., and Dan, Y. (2014). Selective attention. Long-range and local circuits for top-down modulation of visual cortex processing. Science *345*, 660–665.